Diverse styles of submarine venting on the ultra-slow spreading Mid-Cayman Rise

C.R. German[a], A. Bowen[a], M.L. Coleman[b], D.L. Honig[c], J.A. Huber[d], M.V. Jakuba[e], J.C. Kinsey[a], M.D. Kurz[a], S. Leroy[f], J.M. McDermott[a], B. Mercier de Lépinay[g], K. Nakamura[h], J.S. Seewald[a], J.L. Smith[d], S.P. Sylva[a], C.L. Van Dover[c], L.L. Whitcomb[i] & D.R. Yoerger[a]

[a] Woods Hole Oceanographic Institution, Woods Hole MA 02543, USA

[b] NASA Astrobiology Institute & Jet Propulsion Laboratory, California Institute of Technology, Pasadena, CA 91109, USA

[c] Duke University Marine Laboratory, Beaufort, NC 28516, USA

[d] Marine Biological Laboratory, Woods Hole, MA 02543, USA

[e] Australian Centre for Field Robotics, University of Sydney, 2006, Australia

[f] ISTEP, CNRS UMR 7193, Paris, France

[g] CNRS – GéoAzur, Université de Nice-Sophia Antipolis, Valbonne, France

[h] AIST, Tsukuba, Ibaraki 305-8567, Japan

[i] Johns Hopkins University, Baltimore, MD, 21218-2681, USA

CLASSIFICATION

PHYSICAL SCIENCES: Geology

BIOLOGICAL SCIENCES: Microbiology

Abstract

Thirty years after the first discovery of high-temperature submarine venting, the vast majority of the global Mid Ocean Ridge remains unexplored for hydrothermal activity. Of particular interest are the world's ultra-slow spreading ridges which were the last to be demonstrated to host high-temperature venting, but may host systems particularly relevant to pre-biotic chemistry and the origins of life.

Here we report first evidence for diverse and very deep hydrothermal vents along the ~110 km long, ultra-slow spreading Mid-Cayman Rise. Our data indicate that the Mid-Cayman Rise hosts at least three discrete hydrothermal sites, each representing a different type of water-rock interaction, including both mafic and ultra-mafic systems and, at ~5000 m, the deepest known hydrothermal vent. Although submarine hydrothermal circulation, in which seawater percolates through and reacts with host lithologies, occurs on all mid-ocean ridges, the diversity of vent-types identified here and their relative geographic isolation make the Mid-Cayman Rise unique in the oceans. These new sites offer prospects for: an expanded range of vent-fluid compositions; varieties of abiotic organic chemical synthesis and extremophile microorganisms; and unparalleled faunal biodiversity - all in close proximity.

/body

Introduction

The ~50,000km global ridge system, comprising both mid-ocean ridges and back-arc spreading centers, is an integral component of Earth's plate tectonic system. They define the diverging margins of tectonic plates that separate at rates that range from "very fast" (>20 cm/yr) to "ultra-slow" (<2 cm/year). But the distribution of slow or fast spreading ridge systems is not uniform throughout the globe: slow- and ultra-slow ridges dominate the Arctic, Atlantic and SW Indian Oceans, while fast-spreading ridges are only found in the Southern and Pacific Oceans (1). To date, only ~10% of the global ridge system has been explored systematically for hydrothermal activity (2) and it has only recently been recognized that the world's slowest-spreading ridges can host hydrothermal activity (3-6). To a first approximation, the incidence of hydrothermal venting is greatest on fast-spreading ridge systems (2). Slow and ultra-slow spreading ridges comprise 50% of the cumulative global ridge-axis length (1), however, and a greater diversity of *styles* of hydrothermal venting has been found along these slower ridges (7), including vents that derive their chemical signatures, at least in part, from extruded or deep-seated ultramafic rocks (8-11). This is important because the impact of hydrothermal activity on ocean biogeochemistry depends on global vent-fluxes, fluid compositions, *and* where the flux enters the ocean along the global thermohaline conveyor (12). Further, ultramafic-hosted sites such as *Rainbow* or *Lost City* create extremely reducing chemical environments that have the potential to host abiotic organic synthesis relevant to studies of prebiotic chemistry and the origins of life (11, 13).

Here we report results from an investigation into the distribution and nature of seafloor venting along the Mid-Cayman Rise (MCR) and demonstrate the occurrence of diverse styles of hydrothermal activity spanning a broad range of depth, temperature and rock types. The MCR, a ~110 km long, deep (4500-6500 m) and ultra-slow (<2 cm yr^{-1}) spreading ridge, is tectonically and geographically isolated from all other components of the global ridge system (14; Fig.1). It represents a particularly exciting environment to study species dispersion and the evolution of vent organisms due to its location at the deep-water gateway that used to exist between the eastern Pacific and equatorial Atlantic Oceans prior to the closure of the Isthmus of Panama at ~ 3.1 Ma (15). For our work, an instrument package comprising an optical back-scatter sensor to detect suspended particles, an Eh electrode to detect reduced chemical species, and a conductivity, temperature, depth instrument (CTD), was deployed from the deep-diving *Nereus* vehicle (16) and a wire-line rosette equipped with 23 acid-cleaned 10 L Niskin bottles. Using *in situ* sensing, together with ship-board and laboratory analyses of water samples for chemical (Eh, CH_4, ^3He, Fe, Mn) and microbial indicators, were have identified, located and deduced the nature of a series of hydrothermal sources along the MCR.

While hydrothermal vent sites only typically occupy small areas on the seafloor (~100 m across), the plumes formed when hot, acidic vent fluids mix turbulently with cold deep-ocean seawater can rise hundreds of meters through the water column before attaining neutral buoyancy. These plumes can then be detected for kilometers or more away from their source, as they disperse, due to their enrichment in dissolved chemicals, mineral particulate and microbes when compared to the ambient water column (17). To date, three “end-member” vent-types have been identified at mid-ocean ridges. Type 1,

the most commonly reported, is a mafic-hosted, high-temperature system which can occur under neovolcanic (e.g. East Pacific Rise, 9-10°N; 18) or tectonic (e.g. *TAG*, 26°N, Mid-Atlantic Ridge (MAR); 19) control, with end-member fluid temperatures up to 407°C and relatively low dissolved CH_4 concentrations (20) that result in low CH_4:Mn ratios in their overlying plumes (21). Type 2 is a distinct form of high-temperature venting associated with serpentinization of ultramafic rocks (e.g. *Rainbow*, 36°N, MAR), characterized by high H_2, CH_4, and Fe concentrations in the vent fluids (8, 9) and resulting in much higher plume-height CH_4:Mn ratios (12). Type 3 is the most recently identified, from the *Lost City* site, 30°N MAR (10) and also involves serpentinization of ultramafic rock, but yielding substantially lower fluid temperatures exiting the seafloor (~40-90°C). The *Lost City* style of venting is associated with long-lived detachment surfaces that play an important role in extension along all slow spreading ridges (22). Although plume data for *Lost City* are not available, the vent fluids contain CH_4 and H_2 at levels comparable to Type 2 vents, but with much lower dissolved metal concentrations (10, 23). Plumes that have previously been attributed to such a source - at the 15°20'N Fracture Zone, MAR - exhibit extremely high CH_4:Mn ratios and an absence of particulates (24).

Because of the diversity in styles of venting that can occur along slow and ultra-slow ridges, we chose to employ a diverse array of geochemical (Eh, CH_4, ^{3}He, Fe, Mn) techniques for our study of the MCR to ensure that we would be able to both recognize, and distinguish between, water column signals from any Type 1, 2 or 3 vents present. Remarkably, our results provide evidence that one example of all three of these distinct vent-types are currently active on the MCR, all within less than 100km along-axis.

Results & Discussion

Most of the stations that we occupied along and across the MCR (spaced ≤10 km apart, both along the neovolcanic ridge-axis and close to the rift-valley walls (14)) revealed no evidence for any form of hydrothermal discharge (black circles in Fig.1). However, three distinct sites of activity were identified. The first of two extremely deep sites, which we have named *Piccard* and *Walsh* in honor of the deepest diving human exploration of the ocean 50 years ago, lies in the northern half of the MCR (Fig.1). At the *Piccard* site, CTD hydrocasts and *Nereus* surveys detected strong Eh and particulate signals in a double plume, at 3900 m and 4250 m, that were co-registered with positive anomalies in four diagnostic hydrothermal tracers (Fig.2a): total dissolvable Fe (TDFe), dissolved ^{3}He anomaly ($\delta^{3}He = [(^{3}He/^{4}He)_{sample}/(^{3}He/^{4}He)_{air}-1)100)]$), dissolved CH_4 and total dissolvable Mn (TDMn). Microbial cell counts were also enhanced in both plume layers (Fig.2a) reaching concentrations 2-4 times higher (23,000 cells/ml at 4150 m; 34,000 cells/ml at 3950 m) than background values from above plume-height (8,700 cells/ml).

Ratios of CH_4 to Mn at plume-height provide a clear distinction between mafic-hosted (low CH_4:Mn) and ultramafic-hosted (high CH_4:Mn) hydrothermal systems (21, 24). At the *Piccard* site, plume CH_4:Mn ratios are the lowest detected along the MCR (Fig.3a), directly comparable to plume ratios reported from the Type 1, mafic-hosted *TAG* hydrothermal field (26°N, MAR: 21), and consistent with images of basaltic pillow and sheet-flows reported previously from the MCR rift-valley floor (14). The combination of pronounced optical back scatter anomalies together with high

concentrations of both dissolved gases (CH_4, ^3He) and metals (TDFe, TDMn) in the *Piccard* plume provide clear evidence for a source of high-temperature venting on the underlying seafloor. Further, interception of distinct *buoyant* plume signals at this site, at 4400-4500m depth, (Fig.4) allow us to predict the location of the source of venting. Theory that has proven robust in the deep ocean predicts that the turbulent rise of a buoyant hydrothermal plume should approximate to an inverted cone with a half-spreading angle of thirty degrees (26). For example, in recent surveys of previously unexplored sections of Pacific, Atlantic and Indian ridge-crest, autonomous underwater vehicle (AUV) dives have relied on this same approximation to routinely intercept more than ten different buoyant hydrothermal plumes (e.g. 27, 28). Using the same approach here, we can predict that the buoyant plume signals we have intercepted at ~500 m off-bottom must originate at a source of venting - the *Piccard* vent site - that lies within a range of ~250 m from this location (18° 32.687'N, 81°43.170'W) within the red circle projected onto the seabed in Fig.4 and at a depth of ~5000 ± 50 m. Previously, the deepest known hydrothermal field worldwide was the Ashadze site (13°N, MAR), at 4200m depth (http://www.interridge.org/files/interridge/vents_interridge_2009_all.kml). Therefore, this new *Piccard* site, at ~18°33'N on the MCR, represents the world's deepest high-temperature hydrothermal field by ~800 m.

A second set of deep (~3800 m) hydrothermal plume signals were detected at the very southern end of the Mid-Cayman Rise (Fig.1) where *in situ* data from three CTD stations exhibited optical back-scatter anomalies indicative of particle-rich plumes, but no detectable Eh anomalies. For both optical backscatter and CH_4 concentrations, strongest signals were detected at the central station compared to those observed to East and West.

No samples for dissolved δ^3He or microbial analysis were obtained from this *Walsh* site but the depths of maximum TDFe and TDMn concentrations at the central CTD station coincided with maximum optical back-scatter and dissolved CH_4 anomalies at ~3800m (Fig.2b), providing strong evidence that this high-temperature hydrothermal source must also lie at a depth of ≥4000m, representing a second particularly deep seafloor vent-site. When compared to *Piccard*, however, plume-height CH_4:Mn ratios at the *Walsh* site are much higher, consistent with more CH_4-rich source-fluids (Fig 3a). Indeed, CH_4:Mn ratios for the *Walsh* plume are almost identical to those reported for the Type 2, *Rainbow* site (36°N, MAR: 12) leading us to deduce that these plume signals, at the southernmost end of the MCR, most likely derive from a Type 2 high-temperature hydrothermal field hosted in ultramafic rocks. While the absence of Eh anomalies from the plume signals detected (Fig.2b) indicate that none of these southernmost CTD stations approached particularly close to the source of the *Walsh* plume, CTD stations occupied immediately to the north (Fig.1) show no evidence of these same deep plume signals. Consequently, we infer that the *Walsh* high-temperature vent source must lie south of 18°00'S and, from comparison with the geologic setting of other Type 2 sites (*Rainbow, Logatchev, Ashadze*) most probably lies toward the base of the rift-valley wall toward the SE or SW corner of the MCR axis.

The third site that we have identified, *Europa*, was also first detected over the southern MCR, where water samples along the western axis, 18°00'-20'N (Fig.1) exhibited dissolved CH_4 enrichments at ~2100 m depth that decreased from NW (12 nmol L^{-1}) to SE (2 nmol L^{-1}), unaccompanied by *in situ* optical backscatter or Eh anomalies. By tracing this plume north, toward the only section of the MCR shallower

than 2500 m, highest concentrations of dissolved methane (>30 nmol L^{-1}) were detected near 18° 21.5'N (Fig.2). Anomalies in δ^3He, microbial cell counts, and Eh were also observed at this site, but no optical back-scatter or TDMn anomalies and only a slight enrichment in TDFe were observed (Fig.2c). These water-column signals are quite different from the deeper-lying *Piccard* and *Walsh* plumes. Strongest anomalies were observed near the summit of Mt. Dent, a long-lived detachment surface (18°20'-18°25'N) where *Alvin* submersible transects had previously documented outcropping ultramafic rocks (14). The absence of *in situ* optical back-scatter anomalies or high TDFe and TDMn concentrations at this site (Fig. 2c) provides strong evidence that these water column signals do not derive from a high temperature hydrothermal source. Further, the CH_4:Mn ratios at this *Europa* site are substantially elevated over what would be predicted from a Type 1 (e.g. *TAG*, *Piccard*) or Type 2 (e.g. *Rainbow*, *Walsh*) vent. Yet the presence of a marked anomaly in the *in situ* Eh data, together with positive anomalies in the dissolved CH_4, δ^3He and cell-count profiles, indicate that these signals most certainly are hydrothermal in origin. In a prior study at the Endeavour segment, Juan de Fuca Ridge (JdFR; 29) anomalously high hydrothermal CH_4 concentrations were attributed to thermogenic decomposition of organic rich sediments, sub-seafloor. While similar processes could also be active on the Mid-Cayman Rise, the high CH_4 emissions observed in the JdFR study were associated with "black smoker" *high-temperature* vents (29). By contrast our data are only consistent with a *low-temperature* form of hydrothermal circulation. Further, because the methane-rich *Europa* plume signals originate close to the summit of Mt. Dent – a long-lived detachment surface – a more likely explanation may be that they are associated with serpentinization of ultramafic

rocks and, hence, more closely related to low-temperature Type 3 venting as reported previously from *Lost City* (10).

Bacterial community composition was examined in filtered plume water samples from the *Piccard* and *Europa* sites using a 454 tag pyrosequencing approach (30, Supp. Table 1). While most of the taxa detected in those samples originate from deep seawater, there were also some *Epsilonproteobacteria* and *Gammaproteobacteria* indicative of microaerobic, reducing environments in the water column. We did not sample water for DNA analysis that was "true" background seawater; all 5 of the samples we sequenced had elevated methane concentrations (Supp. Table 1). Clustering of sequences at the 3% OTU level (31) followed by hierarchical cluster analysis showed that the two samples from *Piccard* grouped together and two of the three *Europa* samples clustered together, with one outlier (Supp. Fig. 1). The outlying sample, CH0909-08, had a large number of sequences related to *Pseudomonas* and *Burkholderia*, and we suspect it may have been contaminated during shipboard sampling; this sample was not included in further analyses. At the *Piccard* site, there were no discernable differences between the two samples and the most abundant sequence recovered belong to the *Gammaproteobacteria* SUP05, comprising almost 5% of all sequences. This organism was also found as the most dominant bacteria detected in the hydrothermal plume from Suiyo Seamount (32: Fig. 5). SUP05 is related to sulfur-oxidizing gill symbionts of bivalves from deep-sea vents and has also been found in Oxygen Minimum Zones in several of the world's oceans. Metagenomic analysis of the uncultivated SUP05 from water-column redox clines in Saanich Inlet, British Columbia indicates that this organism is capable of

chemolithoautotrophic growth through the oxidation of reduced sulfur compounds (33). SUP05 sequences were also the second-most abundant sequence at the *Europa* site, comprising almost 3% of all sequences. While these sequences have been detected in oxygenated water, they are often abundant in hydrothermal plumes (32, 34). In addition, we detected the genus *Sulfurimonas* of the *Epsilonproteobacteria* at both sites at relatively high abundances (2% of sequences at *Piccard*, 4% at *Europa*). The genus *Sulfurimonas* is associated with environments in which a gradient exists between anaerobic and aerobic habitats. In these redox clines, they can utilize reduced sulfur compounds (sulfide, elemental sulfur, thiosulfate) as electron donors and oxygen as an electron acceptor for chemolithoautotrophic growth (35). *Sulfurimonas* have been detected at hydrothermal vents, in plume samples, and in marine sediments, but not in surface seawater. The dominant *Sulfurimonas* sequence in our MCR samples was an exact match to an uncultured *Sulfurimonas* environmental clone from oceanic crustal fluids in the Southern Mariana Trough (36; Fig.5). Our search of the International Census of Marine Microbes datasets (available at vamps.mbl.edu) for *Sulfurimonas* showed that these sequences are only abundant in reducing environments such as deep and shallow marine hydrothermal vents, methane seeps, and the Black Sea. In deep waters from the Atlantic and Arctic, very few or no *Sulfurimonas* sequences were found, representing much less than 0.1% of total sequences recovered in these samples. The relatively high abundance of *Sulfurimonas* found in our samples (2-4%) suggests a local enrichment of these organisms in the hydrothermal plumes. While we cannot infer the nature of discrete vent *sources* from these microbial data, the enriched cell concentrations and relatively high abundance of organisms that favor redox-active environments in our

plume samples are entirely consistent with our geochemical data that indicate the presence of hydrothermal sources releasing chemically-reducing fluids from the seafloor.

The frequency of venting and diversity of vent styles detected along the ultra-slow spreading Mid-Cayman Rise is remarkable. Previously, it has been argued that hydrothermal activity should be most abundant along the world's fastest spreading ridges where axial magmatic fluxes are highest (2). While that work also acknowledged that there may be more venting on slower spreading ridges than can be accounted for from magmatic heat-flux alone, an earlier study of the comparably deep and ultra-slow spreading Gakkel Ridge (5) led us to anticipate discovery of one high-temperature vent along the entire MCR. Instead, we have found evidence for three hydrothermally active sites including two sites of high-temperature venting, hosted in mafic (*Piccard*) and ultramafic (*Walsh*) rocks, both at depths in excess of 4000 m. One of these, the *Piccard* high-temperature field, has been located precisely on the MCR rift-valley floor at a depth of ~5000 m, some 800 m deeper than all previously known vent-sites. Perhaps our most significant result, however, is the evidence for a third style of venting at the much shallower *Europa* site. The water column signals from this site are rich in CH_4, ^3He and microbes, but show no evidence for high-temperature venting. This site, therefore, may represent a Type 3 (low-temperature ultramafic-hosted) hydrothermal site such as has only been reported once previously, at *Lost City* (10).

The great depth of the *Piccard* site will allow examination of hydrothermal fluids venting at pressures and possibly temperatures beyond the critical point of seawater at 407°C and 298 bar (37). The two southern sites, *Walsh* and *Europa*, show evidence for

being hosted in ultramafic rocks, at high and low temperatures respectively. These may provide new opportunities to study processes of abiotic organic synthesis relevant to prebiotic chemistry and the microbiology of hydrogen-rich systems that serve as analogues for some of the most primitive environments for life on Earth. Vent systems are also celebrated for the high endemicity of the microbial-invertebrate symbioses they support. Study of vent invertebrates and other organisms at all three newly discovered Mid Cayman Rise hydrothermal fields will provide insight into the evolution, dispersion, and isolation of vent taxa with potential to fill in a critical piece of the global biogeography of chemosynthetic organisms.

Materials and Methods

All seawater samples were collected using acid-cleaned 10 L Niskin bottles mounted on a rosette equipped with a SeaBird 9/11+ CTD to measure conductivity, temperature and depth. A hierarchy of sampling was established for all bottles at all stations that followed the order: *i)* He or CH_4; *ii)* microbes; *iii)* metals. To protect against atmospheric contamination and/or loss of dissolved gases, any fluid samples that were to be analyzed for both CH_4 and He isotopes were drawn from replicate Niskin bottles fired at the same depth. All CH_4 analyses were conducted at sea; all other analyses were completed in shore-based laboratories.

Water samples for helium were collected from the Niskin bottles immediately after recovery in clamped copper tubes (~ 13 g of seawater). Dissolved gases were extracted in the WHOI Isotope Geochemistry Facility using standard techniques and transferred into glass break-seal tubes. Helium concentrations and isotopic compositions were determined using a magnetic sector mass spectrometer by comparison to air

standards of the same size as the samples. Full procedural blanks for extraction are approximately 7 x 10^{-10} cc STP ^{4}He and are insignificant. Uncertainties in the analyses, presented in δ^3He notation $\{\delta^3He = [(^3He/^4He)_{sample}/(^3He/^4He)_{air}-1)100]\}$ were typically 0.8 %.

Water samples for CH_4 analysis (20 ml) were drawn from the Niskin bottles in 60 mL plastic syringes. Dissolved CH_4 concentrations were determined by gas chromatography using a Hewlett Packard 5890 II gas chromatograph fitted with a 6-foot 5Å molecular sieve column and a flame ionization detector following a headspace extraction in helium.

For TDMn and TDFe, 500 mL or 1 L samples were drawn directly from the Niskins, unfiltered, into acid-cleaned low-density polyethylene bottles (rinsed three times with sample prior to filling). In the laboratory, these samples were acidified with 1 mL ultra pure nitric acid for 4 weeks prior to analysis, to ensure complete dissolution and desorption from bottle walls of all the metals present. Mn and Fe concentrations were determined following a standard method of organic complexation, solvent extraction and analysis by atomic absorption spectroscopy (38) yielding analytical precisions of better than 5% for both elements.

For cell counts, an 18 mL aliquot of fluid sample was taken from the Niskin bottles, preserved in formaldehyde (3.7% final concentration) in duplicate, stored at 2°C, and counted using epifluorescence microscopy with DAPI. Additional aliqouts (2-3 L) of seawater were filtered through sterile 47 mm-diameter, 0.22 μm-pore-size filters shipboard, flooded with RNA Later, and stored at -80 °C (Supp. Table 1). DNA was extracted from these filters (30) and bacterial community structure characterized by deep

sequencing of ribosomal RNA (rRNA) amplicon libraries (30) using primers that span the V4-V6 hypervariable regions of the rRNA using the Roche titanium amplicon protocol (39). Pyrosequencing reads were passed through quality filters to reduce the error rate (40). Any read containing one or more ambiguous nucleotides was discarded. The expected sample barcode and primer sequences were trimmed from the proximal and distal ends of the reads. Reads lacking a perfect match to the forward primer or a recognizable match to the reverse primer sequence (including rare variants) at either end and reads that could not be unambiguously assigned to a sample were discarded. Sequences were assigned taxonomy using the Global Alignment for Sequence Taxonomy (GAST) process (41), which incorporates the RDP II taxonomy. All sequences from each sample were pooled and OTUs calculated via SLP PWAL (31). Cluster analysis was carried out using Primer-E software (42). Sequences were also submitted to the BLAST search program (available through the National Center for Biotechnology Information) to find closely related sequences to be used in subsequent analyses. Approximately 400 nucleotide bases were used in phylogenetic analyses, with only homologous positions included in the comparisons. The MEGA version 4 package (43) was used to construct distance based neighbor-joining trees. Bootstrap analysis was used to provide confidence estimates for tree topologies. Sequences have been deposited in the VAMPS database (https://vamps.mbl.edu).

Acknowledgements

We thank the Captain and crew of RV *Cape Hatteras* and the *Nereus* technical team for shipboard support and D.P. Connelly and C.M. Sands (NOC, UK) for help with

operations at sea and shorebased TDFe & TDMn analyses. This research was funded through NASA (ASTEP) and WHOI (Ocean Ridge Initiative). The contribution of MLC was carried out as part of his work at JPL, California Institute of Technology, under contract with NASA. The perceptive insights of two anonymous reviewers greatly helped improve this manuscript.

References

1. Sinha MC, Evans RL (2004) Geophysical constraints upon the thermal regime of the ocean crust. *Geophys. Monogr.* 148: 19-62.
2. Baker ET, German CR (2004) On the global distribution of mid-ocean ridge hydrothermal vent-fields. *Geophys. Monogr.* 148: 245-266.
3. German CR *et al*. (1998) Hydrothermal activity along the South West Indian Ridge. *Nature* 395:490-493.
4. Bach W, Banerjee NR, Dick HJB, Baker ET (2002) Discovery of ancient and active hydrothermal systems along the ultra-slow spreading Southwest Indian Ridge 10 degrees – 16 degrees E. *Geochem. Geophys. Geosyst.* 3: Article number 1044.
5. Edmonds HN *et al.* (2003) Discovery of abundant hydrothermal venting on the ultraslow-spreading Gakkel ridge in the Arctic Ocean. *Nature* 421: 252-256.
6. Connelly DP *et al*. (2007) Hydrothermal activity on the ultra-slow spreading southern Knipovich Ridge. *Geochem. Geophys. Geosyst.* 8: Q08013, doi: 10.1029/2007GC001652.
7. German CR, Lin J (2004) The thermal structure of the oceanic crust, ridge-spreading and hydrothermal circulation: how well do we understand their inter-connections? *Geophys. Monogr.* 148: 1-18.

8. Douville E *et al*. (2002) The Rainbow vent fluids (36 degrees 14'N, MAR): the influence of ultramafic rocks and phase separation n trace metal content in Mid-Atlantic Ridge hydrothermal fluids. *Chem. Geol.* 184: 37-48.
9. Charlou J-L *et al*. (2002) Geochemistry of high H_2 and CH_4 vent fluids issuing from ultramafic rocks at the Rainbow hydrothermal field (3614'N, MAR). *Chem. Geol.* 191: 345-359.
10. Kelley DS *et al.* (2005). A serpentinite-hosted ecosystem: the Lost City Hydrothermal field. *Science* 307: 1428-1434.
11. Proskurowski G *et al.* (2008) Abiogenic hydrocarbon production at Lost City Hydrothermal Field. *Science* 319: 604-607.
12. German CR et al. (2010) Export fluxes from submarine venting to the ocean: A synthesis of results from the Rainbow hydrothermal field, 36°N MAR. *Deep Sea Res.* 57: 518-527.
13. Holm N, Charlou J-L (2001) Initial indications of abiotic formation of hydrocarbons in the Rainbow ultramafic hydrothermal system, Mid-Atlantic Ridge. *Earth Planet. Sci. Lett.* 191: 1-8.
14. Ballard RD *et al.* (1979) Geological and geophysical investigation of the Mid-Cayman Rise spreading center: initial results and observations. *Maurice Ewing Series (Am. Geophys. U.)* 2: 66-95.
15. Tunnicliffe V, Fowler CMR (1996) Influence of seafloor spreading on the global hydrothermal vent fauna. *Nature* 379: 531-533.

16. Bowen A *et al.* (2009) Field trials of the Nereus hybrid underwater robotic vehicle in the Challenger Deep of the Mariana Trench. *Proc.Mar.Tech.Soc./IEEE 2009*, http://ieeexplore.ieee.org/stamp/stamp.jsp?tp=&arnumber=5422311&

17. German CR, Von Damm KL (2004) Hydrothermal Processes. *Treatise of Geochemistry* 6: 181-222.

18. Fornari D *et al.* (2004) Submarine lava flow emplacement at the East Pacific Rise 9°50'N: implications for uppermost ocean crust stratigraphy and hyfrothermal fluid circulation. *Geophys. Monogr*. 148: 187-217.

19. Rona PA *et al.* (1986) Black smokers, massive sulfides and vent biota at the Mid-Atlantc Ridge. *Nature* 321: 33-37.

20. Koschinsky A *et al.* (2008) Hydrothermal venting at pressure-temperature conditions above the critical point of seawater, 5°S on the Mid-Atlantic Ridge. *Geology* 36: 615-618.

21. Charlou J-L *et al.* (1991) Different TDM/CH4 hydrothermal plume signatures: TAG site at 26°N and serpentinized ultrabasic diapir at 15°05'N on the Mid-Atlantic Ridge. *Geochim. Cosmochim. Acta* 55: 3209-3222.

22. Escartin J *et al.* (2008) Central role of detachment faults in accretion of slow-spreading oceanic lithosphere. *Nature* 455: 790-795.

23. Proskurowski G, Lilley MD, Kelley DS, Olson EJ (2006) Low temperature volatile production at the Lost City Hydrothermal field, evidence from a hydrogen stable isotope geothermometer. *Chem. Geol.* 229: 331-343.

24. Charlou J-L *et al.* (1998) Intense CH_4 plumes generated by serpentinization of ultramafic rocks at the intersection of the 15°20'N fracture zone and the Mid-Atlantic Ridge. *Geochim. Cosmochim. Acta* 62: 2323-2333.

25. Speer KG, Rona PA (1989) A model of an Atlantic and Pacific hydrothermal plume. *J.Geophys.Res.* 94: 6213-6220.

26. Turner JS (1973) *Buoyancy Effects in Fluids,* Cambridge University Press, New York 368pp.

27. German CR *et al.* (2008) Hydrothermal exploration with the *Autonomous Benthic Explorer. Deep Sea Res.* 155: 203-219.

28. German CR *et al*. (2008) Hydrothermal activity on the southern Mid-Atlantic Ridge: Tectonically and volcanically-controlled venting at 4-5°S. *Earth Planet. Sci. Lett*. 273: 332-344.

29. Lilley MD *et al.* (1993) Anomalous CH_4 and NH_4^+ concentrations at an unsedimented mid-ocean-ridge hydrothermal system. *Nature* 364: 45-47.

30. Huber JA *et al.* (2007) Microbial population structures in the deep marine biosphere. *Science* 318: 97-100.

31. Huse SM, Welch DM, Morrison HG, Sogin ML (2010) Ironing out the wrinkles in the rare biosphere through improved OTU clustering. *Environ Microbiol* 10.1111/j.1462-2920.2010.02193.x)

32. Sunamura M *et al.* (2004) Two *Bacteria* phylotypes are predominant in the Suiyo Seamount hydrothermal plume. *Appl. Env. Microbiol.* 70: 1190-1198.

33. Walsh DA *et al.* (2009) Metagenome of a versatile chemolithoautotroph from expanding oceanic dead zones. *Science* 326: 578-582.

34. Dick GJ, Bradley MT (2010) Microbial diversity and biogeochemistry of the Guaymas Basin deep-sea hydrothermal plume. *Environmental Microbiology* 12: 1334-1347

35. Campbell BJ, Engel.S, Porter ML, Takai K (2006) The versatile ε-proteobacteria: key players in sulphidic habitats. *Nature Rev. Microbiol.* 4: 458-468.

36. Kato S *et al.* (2009) Abundance of *Zetaproteobacteria* within crustal fluids in back-arc hydrothermal fields of the Southern Mariana Trough. *Env. Microbiol.* 11: 3210-3222.

37. Bischoff JJ, Rosenbauer RJ (1988) Liquid-vapor relations in the critical region of the system NaCl-H_2O from 380°C to 415°C – a refined determination of the critical-point and 2-phase boundary of seawater. *Geochim. Cosmochim. Acta* **52**, 2121-2126.

38. Statham PJ (1985) The Determination of Dissolved Manganese and Cadmium in Sea-Water at low nmol/L Concentrations by Chelation and Extraction Followed by Electrothermal Atomic-Absorption Spectrometry. Anal. Chim. Acta. 169: 149-159.

39. Morrison HG, Sogin M (*in progress*) Microbial profiling of environmental samples using V6V4 pyrotag sequencing.

40. Huse SM *et al.* (2007) Accuracy and quality of massively parallel DNA pyrosequencing. *Genome Biol*. 8: R143.

41. Huse SM *et al* (2008) Exploring microbial diversity and taxonomy using SSU rRNA hypervariable tag sequencing. *PLoS Genetics* 4: e1000255.

42. Clarke KR, Gorley RN (2006) PRIMER v6: User Manual/Tutorial. PRIMER-E

43. Tamura K, Dudley J, Nei M, Kumar S (2007) MEGA4: Molecular evolutionary genetics analysis (MEGA) software version 4.0. *Mol. Biol. Evol.* 24: 1596-1599.

Figure Legends

Figure 1: Map of the Mid Cayman Rise showing locations of CTD stations occupied (circles) plus stations for which *in situ* sensor, geochemical and microbial data are shown in Fig.2. (Inset: location of the MCR in the W. Caribbean).

Figure 2: Vertical profiles of hydrothermal tracers at the (a) *Piccard*, (b) *Walsh* and (c) *Europa* sites. Left panels: *in situ* optical back scatter (black), TDFe (red) and δ^3He (blue); Center: microbial cell counts (black) and dissolved CH_4 (red); Right: TDMn (blue) and *in situ* Eh sensor (black).

Figure 3: (a) Dissolved CH_4 vs TDMn distributions for the *Walsh* (red) and *Piccard* (blue) plumes. Solid lines show least-squares linear regressions for each data set; dashed lines show the CH_4:TDMn trends for the high-temperature, ultramafic-hosted Rainbow plume (36°N, MAR; red) and the high-temperature, mafic-hosted TAG plume (26°N, MAR; blue). (b) Dissolved CH_4 vs TDMn for the *Europa* site (black) together with *Walsh* (red) and *Piccard* (blue). Area shown in (a) corresponds to shaded area in (b).

Figure 4. 3-D projection of the CTD-rosette trajectory as it was tow-yo'd across the rift-valley floor near 18° 33'N, MCR. Inset: plot showing the strong positive temperature anomalies detected at 18° 32.687'N, 81°43.170'W. Since neutrally buoyant plumes in the Atlantic are cold and fresh when compared to background (25), it is clear that the CTD-rosette intercepted a *buoyant* plume rising above the seafloor at this site.

Figure 5: Phylogenetic tree as determined by neighbor-joining analyses of 16S rDNA sequences for select *Gamma*- and *Epsilonproteobacteria* and the Cayman plume

sequences. Scale bar indicates the number of nucleotide substitutions per site; bootstrap values above 50 are shown at each internal node.

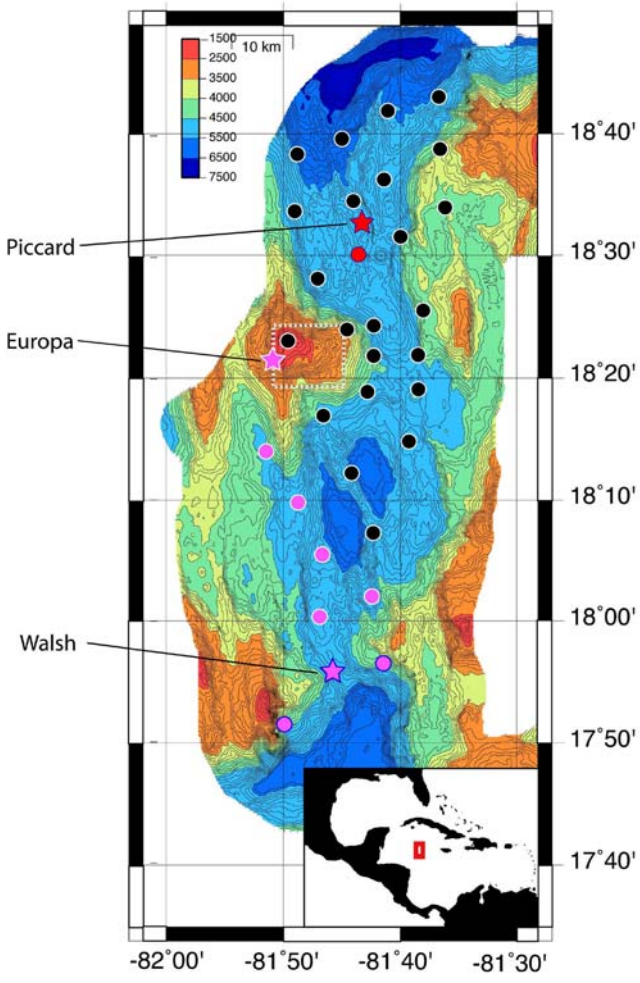
1500
2500
3500
4000
4500
5500
6500
7500
10 km
Piccard
Europa
Walsh
18˚40'
18˚30'
18˚20'
18˚10'
18˚00'
17˚50'
17˚40'
-82˚00'
-81˚50'
-81˚40'
-81˚30'

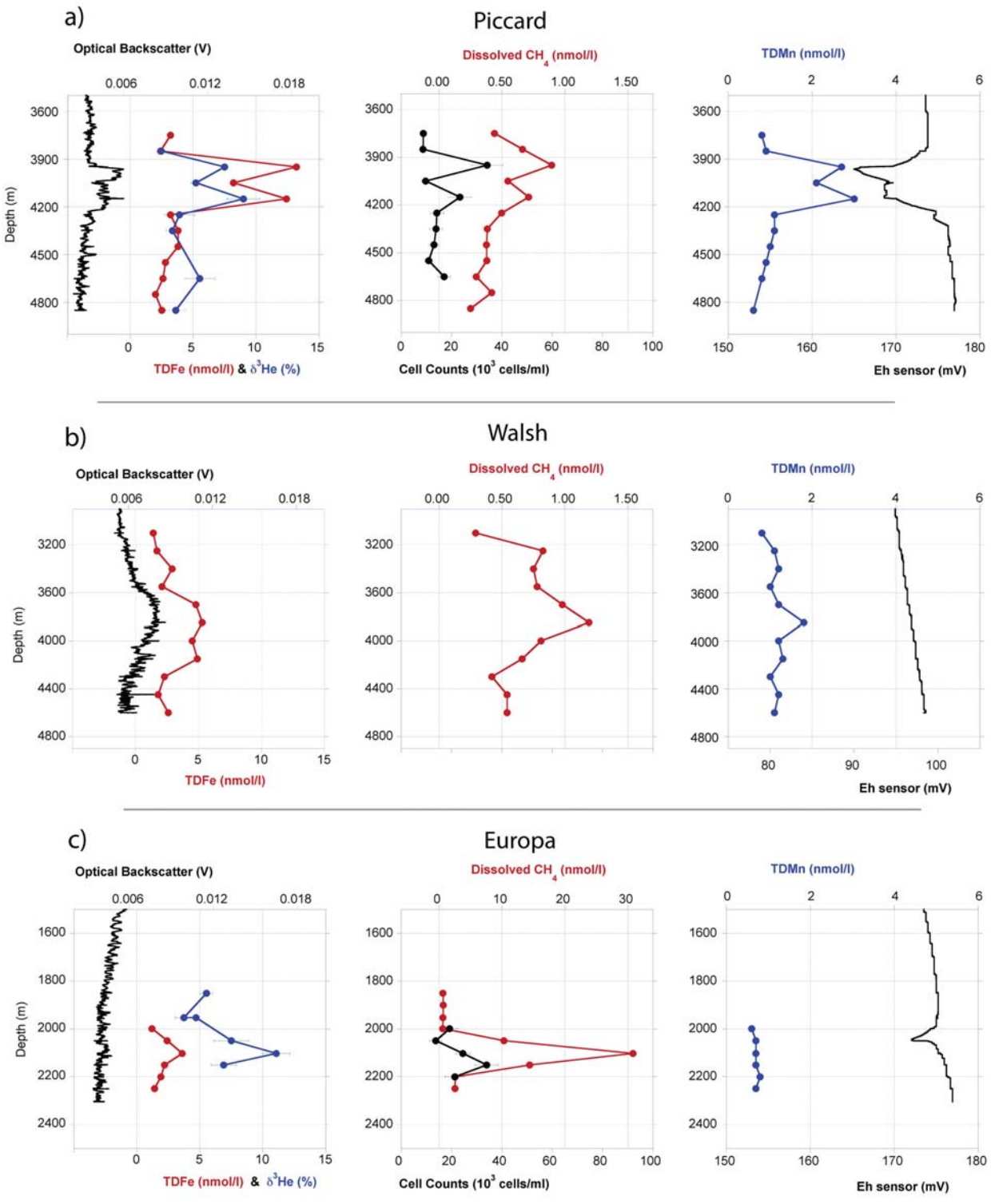
a)
Piccard
Optical Backscatter (V)
0.006
0.012
0.018
Depth (m)
3600
3900
4200
4500
4800
0
5
10
15
TDFe (nmol/l) & δ3He (%)
Dissolved CH4 (nmol/l)
0.00
0.50
1.00
1.50
0
20
40
60
80
100
Cell Counts (10^3 cells/ml)
TDMn (nmol/l)
0
2
4
6
150
160
170
180
Eh sensor (mV)
b)
Walsh
Optical Backscatter (V)
0.006
0.012
0.018
Depth (m)
3200
3600
4000
4400
4800
0
5
10
15
TDFe (nmol/l)
Dissolved CH4 (nmol/l)
0.00
0.50
1.00
1.50
TDMn (nmol/l)
0
2
4
6
80
90
100
Eh sensor (mV)
c)
Europa
Optical Backscatter (V)
0.006
0.012
0.018
Depth (m)
1600
1800
2000
2200
2400
0
5
10
15
TDFe (nmol/l) & δ3He (%)
Dissolved CH4 (nmol/l)
0
10
20
30
0
20
40
60
80
100
Cell Counts (10^3 cells/ml)
TDMn (nmol/l)
0
2
4
6
150
160
170
180
Eh sensor (mV)

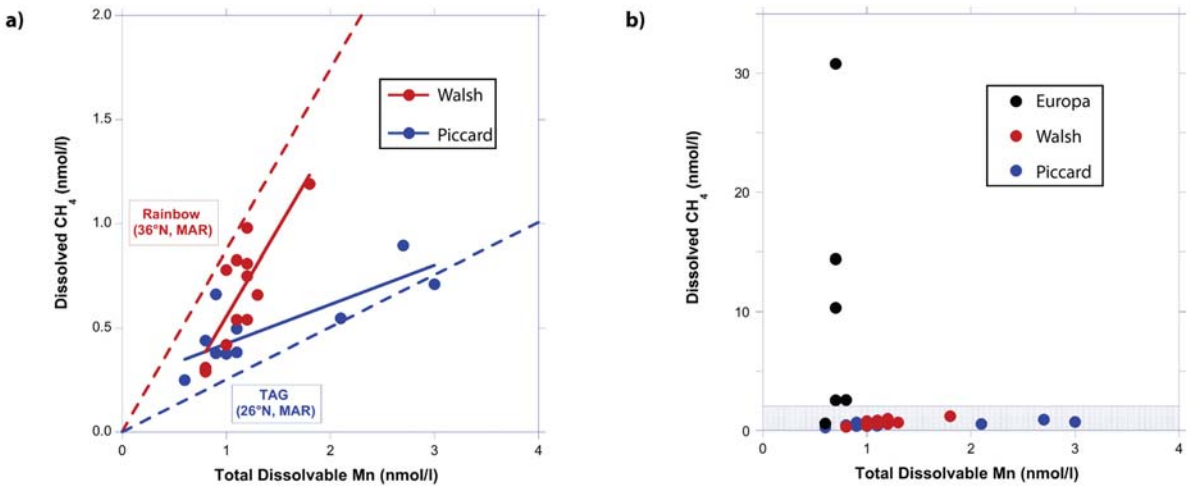
a)
Dissolved CH_4 (nmol/l)
Total Dissolvable Mn (nmol/l)
Walsh
Piccard
Rainbow
(36°N, MAR)
TAG
(26°N, MAR)
b)
Dissolved CH_4 (nmol/l)
Total Dissolvable Mn (nmol/l)
Europa
Walsh
Piccard

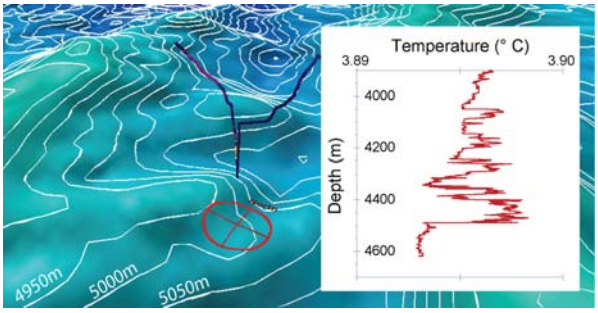
Temperature (° C)
3.89
3.90
4000
4200
4400
4600
Depth (m)
4950m
5000m
5050m

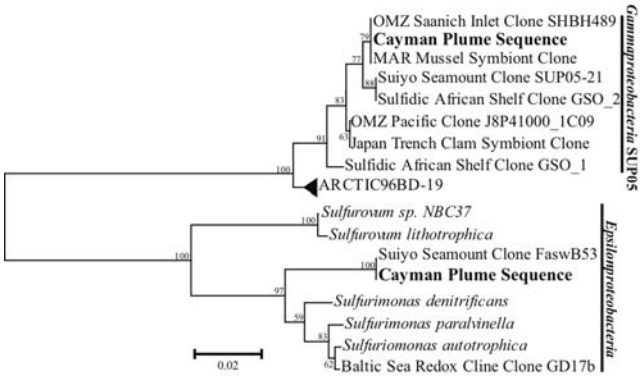
OMZ Saanich Inlet Clone SHBH489
Cayman Plume Sequence
MAR Mussel Symbiont Clone
Suiyo Seamount Clone SUP05-21
Sulfidic African Shelf Clone GSO_2
OMZ Pacific Clone J8P41000_1C09
Japan Trench Clam Symbiont Clone
Sulfidic African Shelf Clone GSO_1
ARCTIC96BD-19
Sulfurovum sp. NBC37
Sulfurovum lithotrophica
Suiyo Seamount Clone FaswB53
Cayman Plume Sequence
Sulfurimonas denitrificans
Sulfurimonas paralvinella
Sulfuriomonas autotrophica
Baltic Sea Redox Cline Clone GD17b
0.02
Gammaproteobacteria SUP05
Epsilonproteobacteria

Supplementary Figure 1 Legend

Cluster diagram at the 3% difference level of all bacteria with each sample labeled according to site.

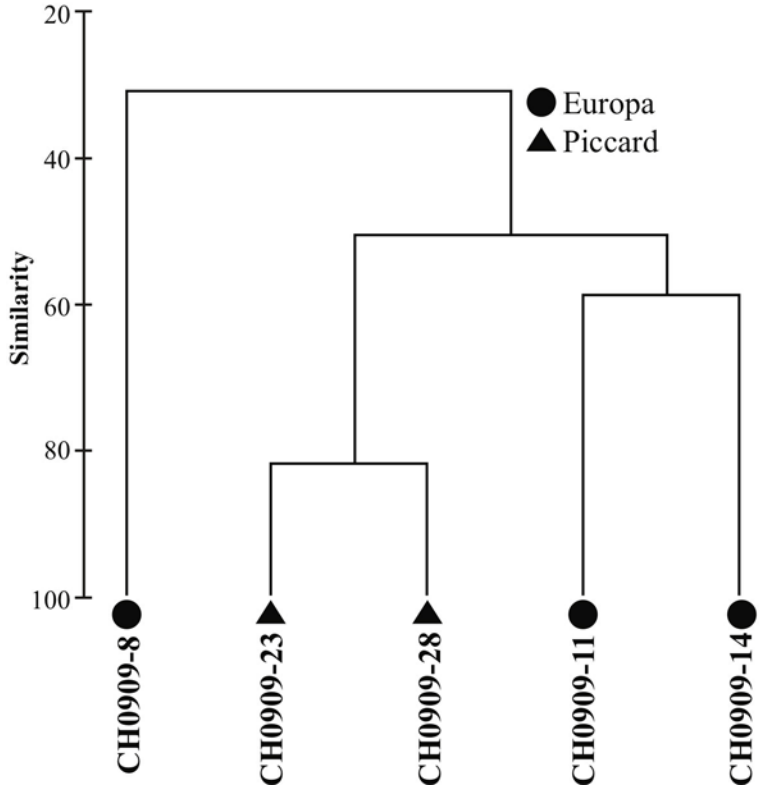
20
40
60
80
100
Similarity
Europa
Piccard
CH0909-8
CH0909-23
CH0909-28
CH0909-11
CH0909-14

Supplementary Table 1

Characteristics of 5 samples used in DNA sequencing analysis

Sample	**Site**	**Depth (m)**	**Cells (ml^{-1})**	**CH_4 ($nmol\ L^{-1}$)**
CH0909-08	Europa	2125	1.56×10^4	10.4
CH0909-11	Europa	2179	1.88×10^4	2.4
CH0909-14	Europa	2023	2.08×10^4	12.5
CH0909-23	Piccard	4650	1.70×10^4	0.3
CH0909-28	Piccard	4150	2.33×10^4	0.7